Progress in Aerospace Sciences 46 (2010) 388–400

Contents lists available at ScienceDirect

Progress in Aerospace Sciences

journal homepage: www.elsevier.com/locate/paerosci

Fluid dynamics and aero-optics of turrets

Stanislav Gordeyev*, Eric Jumper

Department of Aerospace and Mechanical Engineering, University of Notre Dame, 120 Hessert Center, Notre Dame, IN 46556, USA

ARTICLE INFO

Available online 27 July 2010

ABSTRACT

A summary of research efforts for last several years on fluid-dynamics and aero-optics of hemisphere-on-cylinder turrets with flat and conformal windows is presented. The topology of flow behind turrets and both steady and unsteady sources of optical distortions are discussed. Scaling laws for levels of optical aberrations are proposed and results of several experimental studies are compared and discussed. Effects of passive and active flow control in mitigation of aero-optical environment around turrets, as well as current computational studies of aero-optics of turrets are summarized and discussed.

Contents

1. Introduction

From an optical point of view, hemisphere-on-cylinder turrets are optimal platforms with large fields-of-regard to project or receive laser beams to or from a target. Land-based observatories for telescopes are perfect examples of such turrets. But when the turret is placed on an airborne platform moving through the air at subsonic, transonic or supersonic speeds, turrets create complex flow patterns around them. A first-order description of the flow around a turret of this kind is a coherent vortical flow (necklace vortex) in the front stagnation region at the lower cylindrical base with the upper portion of the flow first stagnating than accelerating over the top of the turret; this forward portion of the flow is relatively steady. Then the flow separates from the back portion of the turret forming a complicated highly unsteady wake. These flow phenomena ultimately can impose a number of optically delirious effects on the laser beam projected from the turret. These optical effects are referred to as aero-optical effects [1], but in fact, this classification is itself broken into three distinctive effects: line-of-sight jitter, wavefront aberrations (usually reported with tip/tilt removed) and shock effects. This paper briefly discusses the first and the third types, but primarily discusses the second type of these effects. The atmospheric optical distortions, which effect the beam propagation to the far-field [2], are also outside of the scope of this review.

Airborne optical turrets were extensively studied in the 1970s and early 1980s. For the long-wavelength, around 10 μm, lasers being considered for airborne lasers, these studies showed that, at low speeds, the turrets produce only steady-lensing aberrations and unsteady optical aberrations were found to be a contributing factor only at transonic and supersonic speeds, when unsteady density fluctuations become significant. Good summaries of

* Corresponding author.
E-mail address: sgordeye@nd.edu (S. Gordeyev).

0376-0421/$ - see front matter © 2010 Elsevier Ltd. All rights reserved.
doi:10.1016/j.paerosci.2010.06.001

extensive experimental and modeling studies of optical turrets at transonic and supersonic speeds prior to the mid-1980s can be found in [1,3].

One of the main reasons why turrets were considered optically inactive at low speeds is that the far-field pattern depends on a relative phase distortion, $\phi = 2\pi OPD(x,y,t)/\lambda$, where $OPD(x,y,t)$ is the optical-path-difference of a distorted wavefront, $OPD(x,y,t) = \int n'(x,y,z,t)\,dz$, where n' is the fluctuating index-of-refraction and the integral is taken along the beam's path [4] and λ is the laser wavelength. The fluctuating index-of-refraction, n', is related to the fluctuating density field, ρ', via the Gladstone–Dale constant, K_{GD}, as $n' = K_{GD}\rho'$.[5]. This "constant" depends on the gas mixture and the laser wavelength [6]; for air over the visible-to-IR wavelength range K_{GD} is appoximately $2.27 \times 10^{-4}\,m^3/kg$, increasing slightly for the shortest wavelengths in this range.

A measure of the effect of optical aberrations caused by the flow is to examine its effect on the focusality of the laser in the far-field; this measure is usually expressed in terms of a Strehl ratio, SR, which is the tilt-removed, on-axis, far-field intensity of the aberrated beam divided by that of the unaberrated, that is, the diffraction-limited beam. The large-aperture-approximation [7,58] provides an approximation for SR

$$SR(t) = \exp(-(2\pi OPD_{rms}(t)/\lambda)^2), \quad (1)$$

where $OPD_{rms}(t)$ is the spatial root mean square of $OPD(x,y,t)$.

As mentioned earlier, airborne lasers under consideration during the 1970s and 1980s had wavelengths around 10 μm. Toward the end of 1980s, advances in laser technology made near-IR lasers (with wavelengths ~1 μm) good candidates to be used for airborne lasers. So, while *absolute* optical distortions are relatively small around turrets at moderate subsonic speeds (OPD_{rms}~0.1 μm), *relative* phase distortions, $2\pi OPD_{rms}/\lambda$, imposed on much shorter wavelength laser beams, were increased ten-fold or so, thus making unsteady optical distortions caused by a separated flow behind a turret large enough to significantly reduce the far-field intensity.

In addition, there has been steady progress in wavefront measurement instrumentation. Now wavefront sensors can accurately measure wavefronts as low as a hundredth of a micron at sampling rates of up to ~100 kHz with good (thousands of sub-apertures) spatial resolution. Also, some sensors can measure other important aerodynamic properties like the convective speeds of the aberrating structures in the flow [8,9]. All these reasons have lead to renewed interest in studying and mitigating optical aberrations caused by turrets.

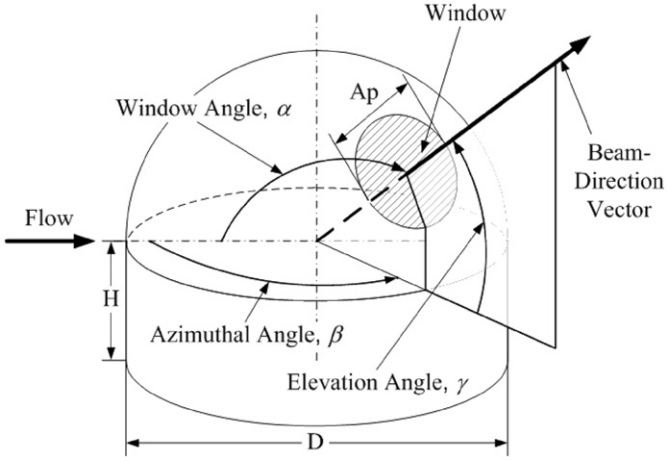

Fig. 1. Definitions of geometric parameters and angles for a hemisphere-on-cylinder turret.

This paper summarizes and analyses recent efforts to investigate the fluid dynamics (Section 2) and aero-optical environments (Section 3) around wall-mounted hemisphere-on-cylinder turrets with either conformal or flat windows at moderate Mach numbers between 0.3 and 0.5. In addition, results for a hemisphere-only turret are given. A short discussion of beam jitter effects and flow topologies around turrets at transonic and supersonic flows is also provided. The latest results in improving optical aberrations via active or passive flow control (Section 4) are summarized and discussed. Finally, a brief summary of computational efforts to predict aero-dynamical and aero-optical properties around turrets (Section 5) is given.

Nose-mounted turrets are not included in this review and the interested reader is referred to [10] for nose-mounted turret issues.

2. Fluid dynamics of turrets

To begin, Fig. 1 shows some basic definitions of the turret parameters and angles. The turret is defined by its hemispherical diameter, D, and the cylindrical base height, H. The diameter of a round aperture window is denoted as A_p. The direction of the outgoing laser beam emerging from the window relative to the incoming freestream flow is typically characterized by the azimuthal and the elevation angles, β and γ, respectively. As will be discussed later in the paper, there is a distinct paucity of optical data; however, we have found it helpful in collapsing the data to define a window angle, α, which is the angle between the outward beam-direction vector, normal to the window center and the freestream-direction vector, pointing upstream, see Fig. 1. The relation between these angles is

$$\cos(\alpha) = \cos(\beta)\cos(\gamma) \quad (2)$$

When the azimuthal angle is zero, the window angle coincides with the elevation angle, $\alpha = \gamma$ and if $\beta = \pi$, then $\alpha = \pi - \gamma$; thus the window angle α goes from 0 to π when the beam-direction vector lies on the center plane, defined as $\beta = 0$ or π. The window angle will be used in the paper to compare optical results between different turrets for different azimuthal and elevation angles.

As mentioned in Section 1, the non-optimal aerodynamic shape of turrets creates a complex flow pattern around the turret, see Fig. 2. It should be noted that this description of the flow has evolved from what we presented in earlier paper [11]; this evolution in better understanding of the global topology of the flow is now based not only on surface visualization, but also working closely with computational fluid dynamicists; some results are reported in Section 5. The flow field consists of a

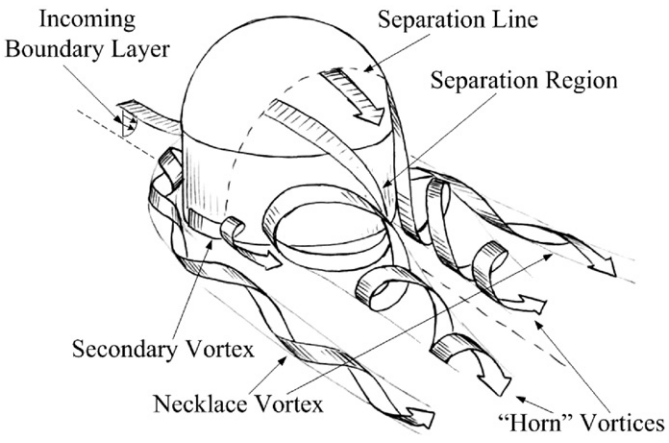

Fig. 2. Schematic of the subsonic flow around the turret.

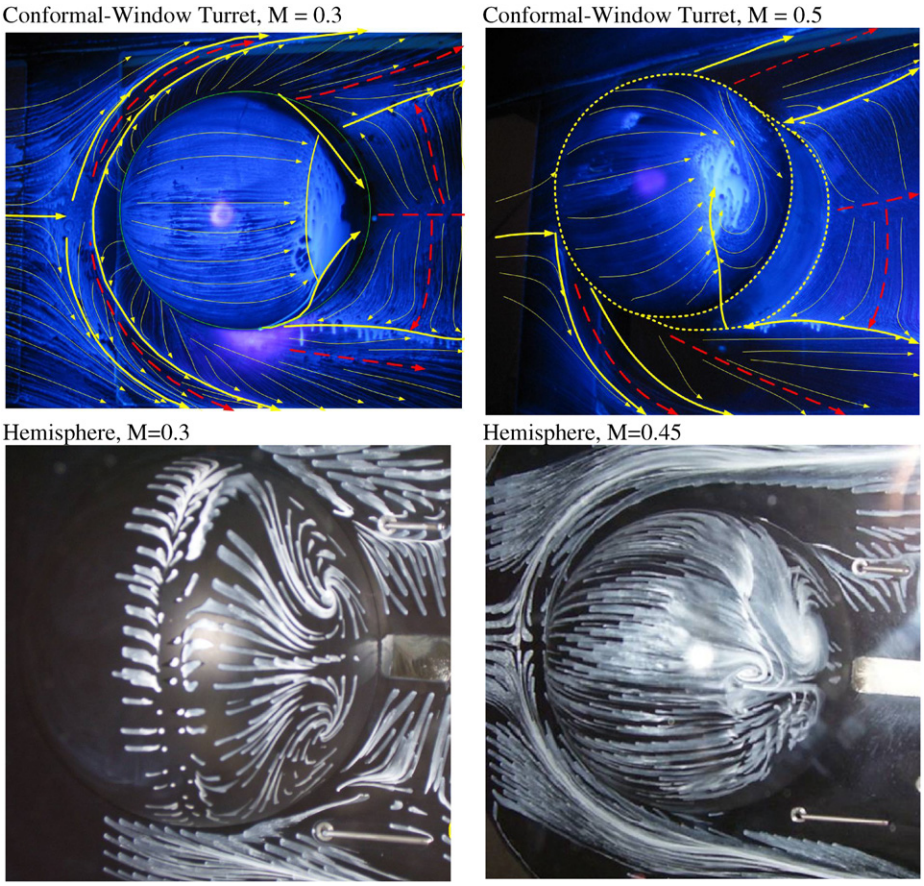

Fig. 3. Surface flow topology on different turrets: conformal window turret at $M=0.3$, $Re_D=2.3\times10^6$ (upper left) and $M=0.5$. $Re_D=3.9\times10^6$ (upper right) (from [17]) and hemisphere at $M=0.3$, $Re_D=2\times10^6$ (lower left) and $M=0.45$, $Re_D=2.9\times10^6$ (lower right) (from [18]).

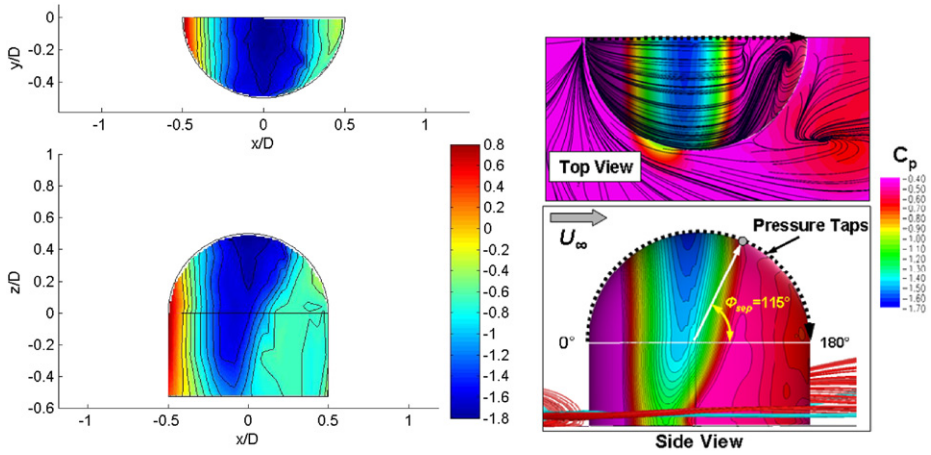

Fig. 4. C_p-distribution on hemisphere-on-cylinder, top (upper plots) and side (lower plots) views. Left: experimental results from [13], $D=10''$, $H/D=0.5$, $Re_D=0.55\times10^6$, flow goes from left to right. Right: computational results from [14], $D=12''$, $H/D=0.375$, $Re_D=2.3\times10^6$.

necklace vortex formed in front of the turret, with its "legs" extending downstream of the turret. The flow is attached at the front part of the turret, while the adverse pressure gradient at the aft part of the turret forces the flow to separate. The separation region interacts with the necklace vortex and creates a complex three-dimensional region behind the turret, with the reversed flow downstream and at the bottom of the turret, as well as secondary vortices on both sides of the turret. The surface-flow topologies around the conformal-window turret and the hemisphere (i.e., $H=0$) at different Mach numbers are shown in Fig. 3. At low Mach numbers, see Fig. 3, left column, two counter-rotating vortices separating from the back part of the turret are clearly visible. At higher Mach numbers, the symmetry between these two vortices is broken and an even-more complex flow pattern at the back of the turret emerges, with either one large or several smaller vortices separating from the back of the turret, visible in Fig. 3, right column. The upstream-moving flow is also clearly visible just downstream of the turret.

When the hemispherical part of the turret is well above the necklace vortex, the flow around the hemispherical section can be approximated by the flow around a sphere. The subsonic flow around spheres at high Reynolds numbers has been extensively

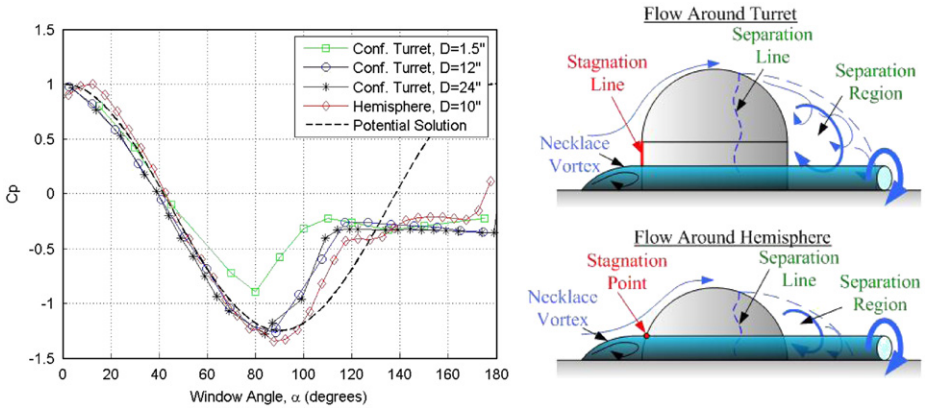

Fig. 5. Left: pressure coefficients along the turret's center-plane, compensated for blockage, for conformal-window turret, $D=1.5''$, $H/D=0.3$, $Re_D=190{,}000$ (from [16]), conformal-window turret, $D=12''$, $H/D=0.375$, $Re_D=2.3\times10^6$ (from [17]), conformal-window turret, $D=24''$, $H/D=0.31$, $Re_D=4.5\times10^6$ (from [15]) and hemisphere, $D=10''$ $Re_D=2.6\times10^6$ (from [18]). The potential solution for the flow around a sphere, Eq. (3), is given as a dashed line. Right: the schematic of the flow topology around the hemisphere-on-cylinder turret and the hemisphere.

studied [12]. It was found that when Re is less than 200,000, the boundary layer is laminar before separation and the separation occurs around a window angle of 80–85°. When the Reynolds number is above 300,000, the separation point over a sphere moves to approximately 120° due to a laminar-to-turbulent boundary-layer transition upstream of the separation point.

Experimental data of the static pressure distribution over the full surface of conformal-window turrets at moderate Reynolds numbers [13] are presented in Fig. 4, left. The results of the computational studies of the turrets [14] are shown in Fig. 4, right, for comparison. Overall, the static pressure distributions are quite similar. The flow speed reaches its highest value on top of the turret; the flow separates around 90° near the bottom of the turret, with the separation point moving further downstream as the height or elevation angle increases. This trend was also observed in other turret studies [15]. The previously mentioned experimental study [13] found that the flow along the centerline of the turret separates around 135°, while other experimental and computational studies at higher Reynolds numbers (discussed in detail later) reported the separation point to be around 115–120°. The relatively high blockage reported in [13], as well as the moderate Reynolds number of 500,000 might be responsible for this anomalously high separation angle.

Surface static pressure measurements along the centerline for different conformal-window turrets are presented in Fig. 5, left. C_p-data for a small turret [16] with $Re_D=190{,}000$ revealed that laminar-boundary-layer separation occurs around 100°, which is somewhat further downstream of the separation point at 82° observed over spheres [12]. Results for pressure distributions at high Reynolds numbers for a turret size, $D=12''$, $H/D=0.375$, $Re_D=2.3\times10^6$ M [17] and $D=24''$, $H/D=0.31$, $Re_D=4.5\times10^6$ [15] are also shown in Fig. 5, left. The C_p-distributions are nearly identical and independent of the Reynolds number. The flow stagnates at the turret front at $\alpha=0°$, accelerates on the front portion of the turret, starts decelerating at the back portion and separates between 115 and 120°, consistent with the separation location over spheres at similar Reynolds numbers. In the separated region the pressure is nearly constant at $C_p=-0.3$, regardless of the Reynolds number. This value is also quite similar to the static pressure inside the separation region reported behind a sphere.

When only the hemisphere is placed on the surface [18], i.e., $H=0$, the presence of the necklace vortex changes the C_p-distribution around the hemisphere, see Fig. 5, left. At first glance, this might be interpreted as improving the aero-optic environment, i.e., the flow appears to be attached longer; however, as discussed in Section 3, the beam must not only propagate through the attached flow, but the more complicated wake [19]. Also, for the hemisphere the near-surface vortical flow structures are closer to the laser beam path, indirectly affecting it via Biot–Savart law. Side-views of the flow topology around the hemisphere-on-cylinder turret and the hemisphere-only are given in Fig. 5, upper and lower right, respectively. For the hemisphere-only, the necklace vortex pushes the stagnation point in front of the hemisphere to approximately $\alpha=15°$, see C_p-distribution in Fig. 5, left. Similar results were also observed by other researchers [13]. The C_p-value on top of the hemisphere ($\alpha=90°$) is slightly lower than on top of the hemisphere-cylinder turret. The flow also separates around 120°, but the C_p-values are not constant inside the separated region, although C_p eventually reaches the same value as for the hemisphere-cylinder turret of $C_p=-0.3$ for $\alpha>140°$.

In Fig. 5, left, the C_p-distribution for potential flow around the sphere,

$$C_p(\alpha)=1-9/4\sin^2(\alpha), \tag{3}$$

is also plotted. For the hemisphere-cylinder configuration, the necklace vortex is well below the hemispherical part of the turret and the potential C_p-solution Eq. (3) describes well the pressure distribution on the front part of the turret. For the hemisphere-only, as mentioned before, the necklace vortex is present at the bottom of the hemisphere, thus slightly changing the C_p-distribution at the front portion from that of the potential solution.

While the static pressure results at the front portion of the hemisphere-on-cylinder turrets along the center-plane are very similar to the results over spheres for high Re numbers, due to the presence of the surface and the necklace vortex at the bottom of the turret, the separated region behind the turret cannot be simply modeled as the separated region behind a sphere. The surface-flow topology on turrets, presented in Fig. 3, clearly indicates the presence of large-scale vortices separating from the back of the turret. The separation line depends on the height or the elevation angle, see Fig. 4, while it stays constant for spheres. Finally, we know that the critical Reynolds number, based on sphere diameter, for laminar-to-turbulent boundary layer transition on a sphere is reported to be ~300,000 [12], and we have seen data, as reported earlier, that shows that transition on a turret is at essentially the same Reynolds number, while other turrets studies have shown transition at Reynolds numbers as high as 500,000; this is mentioned here as a precautionary note, in

attempting to extrapolate data from just over 300,000 to higher Reynolds number applications.

In the case of flat-window turrets the flow becomes viewing-angle-dependent due to the slope discontinuity around the window, thus adding an extra layer of complexity to an already complicated flow topology behind turrets. Unfortunately, only few limited open literature experimental studies of the flow topology (and aero-optical properties) around flat-window turrets are available [1,8].

3. Optical results

The turret changes both the steady and the unsteady components of the density field around it and they will impose steady and unsteady wavefront components on the outgoing laser beam. The time-averaged mean density field will create a *pseudo-steady-lensing* component, usually characterized by a defocus, coma, astigmatism and other low-order Zernike modes. The pseudo-steady-lensing wavefront changes the mean shape of the far-field beam. The unsteady portion of the density field imposes the unsteady aberrations on the beam, forcing it to change its shape and position in time. Often, it is convenient to split these unsteady aberrations into an unsteady tip/tilt or *line-of-sight jitter* and high-order components. These high-order components cause the beam to rapidly change its shape and even to break it into several spots.

To improve the far-field intensity on the target, the damaging effect from all three components on the far-field beam should be reduced by either manipulating the flow around the turret or by applying conjugate wavefronts using an adaptive-optics system [20]. While correcting for the pseudo-steady lensing and the unsteady jitter is a relatively straightforward task for most of commercially available adaptive-optical systems with deformable and fast-steering mirrors, a compensation of the high-order unsteady part of the wavefront with high spatial and temporal frequencies is still outside of current capabilities of these systems.

3.1. Forward-looking angles

As discussed in the previous section, flow around a forward half of the conformal-window side-mounted turret (or nose-mounted turrets [10]) is attached and it can be fairly accurately described by a potential inviscid flow solution around a sphere

$$u_r(r,\alpha)=U_\infty\sin(\alpha)\left[1-\left(\frac{R}{r}\right)^3\right],\quad u_\alpha(r,\alpha)=-U_\infty\cos(\alpha)\left[1+\frac{1}{2}\left(\frac{R}{r}\right)^3\right], \tag{4}$$

where u_r and u_α are the radial and the window-angle velocity components, r is the distance from a point in the flow from the sphere center, U_∞ the freestream velocity and $R=D/2$ the sphere radius. Knowing the velocity distribution in space, the density variations can be estimated assuming weakly compressible flow; the velocity field creates pressure variations through Bernoulli equation, $p'+1/2\rho_0(u_r^2+u_\gamma^2)=p_0=\text{const}$ and the density and pressure are related via an isentropic equation, $\gamma\rho'/\rho_0=p'/p_0=p'/(\rho_0c^2)$, where c is a speed of sound. Finally, the density field can be integrated along the lines parallel to the beam-propagation direction starting at the aperture to get pseudo-steady-lensing, i.e., the optical aberrations due to a steady density field around the turret

$$\begin{aligned} OPD_{steady} &\sim K_{GD}\int_a^\infty \rho'(\vec{x})\,dl \sim -K_{GD}\left(\frac{1}{2c^2}\rho_0\right)\int_a^\infty u^2(\vec{x})\,dl \\ &\sim -K_{GD}\left(\frac{U_\infty^2}{2c^2}\rho_0 R\right)\int_a^\infty f(r/R,\alpha)d(l/R) \\ OPD_{steady} &= (\rho_0/\rho_{SL})M^2Df(Ap/D,\alpha) \end{aligned} \tag{5}$$

where $f(A_p/D,\alpha)$ is a function of the relative aperture size and the window angle. It follows from Eq. (5) that the pseudo-steady-lensing optical aberrations scale as $OPD_{steady}\sim\rho_0M^2D$. Examples of "normalized" wavefronts, $f(A_p/D,\alpha)$, for several forward-looking window angles in the center-plane for $A_p/D=0.33$ are shown in Fig. 6. For simple turret geometries, including the hemisphere only (i.e., $H=0$), the potential approach, Eq. (4) has been extended to transonic and supersonic flows [21] to calculate the pseudo-steady-lensing aberrational environment.

The proposed potential approach fails to take into account optically aberrating effects of sharp density gradients caused by shocks, which, as it will be shown later, are present around the turret at high transonic and supersonic speeds.

Although the flow is attached to the turret's surface for forward-looking angles, optical aberrations, in addition to the pseudo-steady-lensing, also have unsteady components. The laser beam is transmitted *directly* through the attached boundary layer, which itself has been shown to be a source of unsteady optical aberrations at high subsonic speeds [22–24]. The second source of unsteadiness is the necklace vortex at the bottom of the turret and the unsteady separated region behind the turret, which *indirectly* affect the pressure and density field *everywhere* around the turret via a Biot–Savart induction mechanism; the necklace vortex is somewhat unsteady and it has been shown that its movement can be correlated to the unsteadiness in the wake. Evidence of these indirect effects on the optical aberrations has been experimentally observed around the conformal-window turret [17].

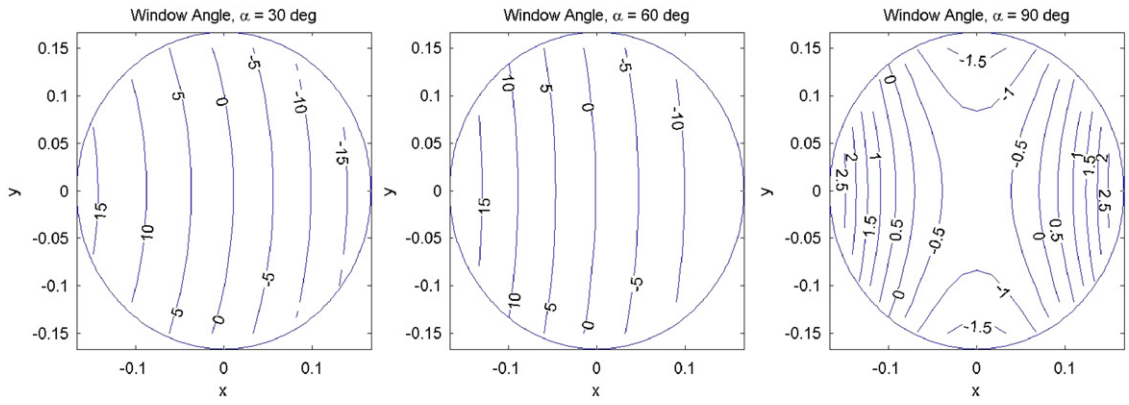

Fig. 6. Steady lensing normalized wavefronts, defined in Eq. (5) for several forward-looking window angles around the sphere.

The flow around the flat-window turret is more complex due to the surface-slope discontinuity around the aperture window, so the potential solution approach, Eq. (5), will not work to estimate pseudo-steady-lensing effects for forward-looking angles. Also, the slope discontinuity can create local separation/re-attachment regions over the flat window for side-looking viewing angles, which is an additional source for unsteady optical aberrations. This effect is yet to be experimentally studied to any depth, although some detailed studies have been carried out for a "cylindrical turret" with a flat window [25,26], see Section 6. Optically, the limited data on flat-windowed turrets bear similarity to the cylindrical, flat-window turret [27].

The pseudo-steady-lensing effect is also present for back-looking angles, but due to the presence of the separated region behind the turret the analytical estimation becomes difficult and therefore this effect should be measured experimentally or calculated numerically.

3.2. Back-looking angles

When the beam is directed backward, it is transmitted through the separated region behind the turret. For large turrets at high Reynolds numbers, the separation occurs around 115–120°, so for window angles around or above these values, large-scale vortical structures inside the separated shear layer become the main source of the unsteady optical distortions and severely limit the performance of turret-based lasers at back-looking angles.

It is often assumed that the both pseudo-steady-leasing and the jitter component of the wavefront can be corrected using an adaptive-optical system, so everywhere later in this paper we consider the high-order unsteady portion of the wavefront only.

To properly analyze experimental results, it is important to understand the scaling of these unsteady aberrations. Recall that optical path difference, *OPD*, is proportional to the integral of the density variations through the turbulent field, $OPD(x,y,t) \sim \int \rho'(x,y,z)\,dz$. For isentropic flows, $p'/p_0 \sim \gamma\rho'/\rho_0$, where ρ_0 and p_0 are freestream density and pressure, respectively. Noting that the pressure drop inside a vertical structure of size θ with a characteristic velocity u is $\Delta p \sim \rho_0 u^2 \sim p_0/T_0 u^2 \sim p_0(u/c)^2 \sim p_0 M^2$, we get the following expression for the variations in *OPD*:

$$OPD_{rms} \sim \theta\rho_0 M^2,$$

where M is the convective Mach number and c a freestream speed of sound. Thus, optical aberrations due to vortical structures depend linearly on the freestream density and the structure size and the square of the convective Mach number. This 'ρM^2'-dependence of the level of optical distortions has been repeatedly shown to be correct for most of the turbulent flows at subsonic speeds [8,17,18,24,30].

In general, optical aberrations depend on the incoming-boundary layer thickness, δ, a typical vortical structure size/scale, θ, the turret diameter, D, the cylindrical base height, H, the beam aperture, A_p, the freestream density, ρ_0, the freestream Mach number, M, the Reynolds number, Re, the window type (flat or conformal) and the viewing angles, α and γ.

$$OPD_{rms} = f(\delta,\theta,D,H,A_p,\rho_0,M,Re,\alpha,\gamma,\delta). \tag{6}$$

Using Eq. (6) and applying dimensional analysis, we can get the following relationship for the OPD_{rms},

$$\frac{OPD_{rms}}{D} = \frac{\theta}{D}\frac{\rho_0}{\rho_{SL}}M^2 g\left(\frac{A_p}{D},\frac{\delta}{D},\frac{H}{D},\alpha,\gamma,Re\right) \tag{7}$$

For a sufficiently small incoming boundary layer, $\delta/D \ll 1$, most of the boundary layer on the turret-mounting surface upstream of the turret gets wrapped into the necklace vortex and does not *directly* affect optical distortions over the turret. A new boundary layer on the hemispherical portion of the turret starts re-growing from the stagnation point in front of the turret. Therefore, the boundary-layer thickness before it separates from the turret will be proportional to the turret diameter only; therefore, the large-scale structures inside the separated shear layer, θ, will also be proportional to the turret diameter, $\theta/D \cong$ const.

When the Reynolds number is smaller than the critical number, $Re < Re_C$, the boundary layer on the turret is laminar and the separation point is located around $\alpha = 100°$. When $Re > Re_C$, the boundary layer becomes turbulent before it separates and the separation point moves to approximately $\alpha = 115$–$120°$, see Fig. 5. The main mechanism for creating the large-scale structures inside the separated shear layer, which have been shown to be the main source for the optical distortions [27,28], is the inviscid inflectional mechanism, which is mostly independent of *Re*; the Reynolds number affects only the small structures in the shear layer which typically do not add any significant optical distortions when compared to the distortions caused by the separated-flow structures. Therefore, as long as the Reynolds number is greater than the critical value, the optical distortions are assumed to not be dependent on *Re*. Therefore, the proposed scaling in Eq. (7) can be re-written as

$$\frac{OPD_{rms}}{(\rho_0/\rho_{SL})M^2 D} = A\left(\frac{H}{D},\frac{A_p}{D},\text{geometry}\right)B(\alpha,\gamma) \tag{8}$$

where A is a function of the turret base height, H/D, and the turret type (i.e., flat window versus conformal window), as well as the relative aperture size, A_p/D. If the relative aperture size is the same between different experiments, A becomes a function of the turret height and type only. B is a function of the window viewing angle only.

For back-looking angles, $\alpha > 90°$, the laser beam travels a longer distance through the separated region of the flow behind the turret, and it is reasonable to assume that the optical aberration will be proportional to this distance. As a first

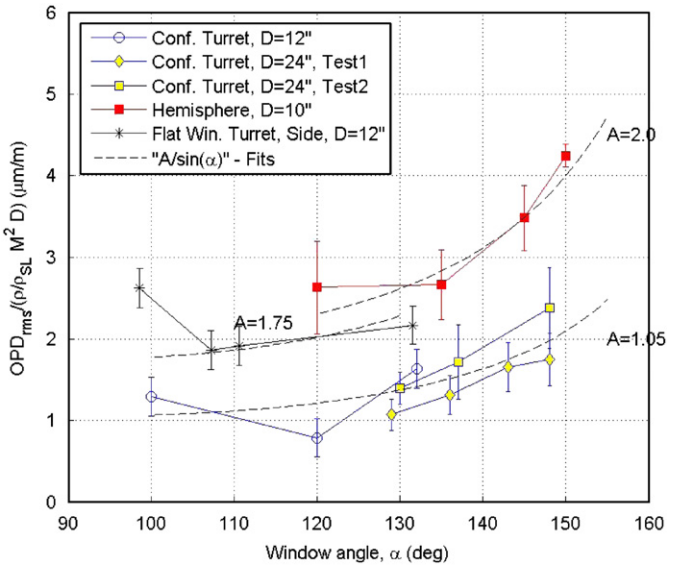

Fig. 7. Levels of optical distortions, OPD_{rms}, normalized by $(\rho/\rho_{SL})M^2 D$ for different turrets as a function of the window angle, α, defined in (1): conformal-window turret, $D=12''$, $H/D=0.375$, center-plane, Shack–Hartmann WFS (from [17]), conformal-window turret (test 1), $D=24''$, $H/D=0.31$, center-plane, Malley Probe (from [30]), conformal-window turret (Test 2), $D=24''$, $H/D=0.31$, center-plane, Shack-Hartmann WFS (from [31]), hemisphere, $D=10''$, $H/D=0$, center-plane, Malley Probe, (from [18]) and flat-window turret, $D=12''$, $H/D=0.375$, $\gamma=30°$, Shack-Hartmann WFS (from [27]). Aperture size is 1/3 of the turret diameter for all cases. "$A/\sin(\alpha)$"-fits are shown as dashed lines with different constants A, defined in Eq. (8).

approximation, the elevation-angle-dependence can be neglected, i.e., $B=B(\alpha)$ in Eq. (8); moreover, it has been proposed that $B=1/\sin(\alpha)$, similar to the observed oblique-viewing-angle dependence, observed for the turbulent boundary layers [23] and separated shear layers [29].

To check the proposed scaling of Eq. (8), optical results from several tests for different turrets with different shapes (conformal window [18,30,31], flat window [27]) and different H/D over a range of back-looking angles are plotted in Fig. 7. The relative window aperture was the same for all turrets, $A_p/D=0.33$. All optical results were corrected for the tunnel blockage. "$A/\sin(\alpha)$" —fits are also plotted in Fig. 7 for different experiments. The "oblique-angle" approximation, $1/\sin(\alpha)$, at least empirically, provides a good fit to all the available data. Clearly, the function A depends on the turret geometry: $A=1.05$ μm/m for the conformal-window turrets, $A=1.75$ μm/m for the flat-window turrets and $A=2.0$ μm/m for the hemispheres only, i.e., $H=0$.

Several important observations can be drawn from Fig. 7. First, somewhat contrary to a conventional thinking, the less-protruding hemisphere-only turret provides the worst optical environment, while the more-protruding hemisphere-on-cylinder turret (with $H/D=0.33$) is almost twice better aero-optically. One possible explanation is that for the hemisphere-only, the necklace vortex is closer to the aperture window and has a greater indirect effect on the laser beam, see Fig. 5, lower right.

Another observation is that the flat-window turret is always aero-optically worse than the conformal-window turret, although there is no experimental data available to see whether optical aberrations for the flat-window turret and the conformal-window turret would converge for large window angles above 150°, when the flat-window aperture is completely inside the separated flow behind the turret.

It is important to note the accuracy of optical measurements and choice of the sensor to collect the optical data. The optical measurements were performed on the same conformal-window turret over the same range of window angles during two separate tests, one with the Malley probe [30] and another with a Shack–Hartmann sensor [31]. Results presented in Fig. 7, indicate slightly different values, although agreeing with each other within the error bounds of either sensors. Detailed analysis of main wavefront corrupting effects for different wavefront sensors and means to remove them is presented in [31]. Due to different wavefront corrupting effects, it is very useful to use a suite of different optical instruments to obtain reliable optical data.

The final note about the optical environment around different turrets for back-looking angles is that Fig. 7 presents almost all data available in the open literature; yet, there are only 10 points for the conformal-window turrets along the center-plane, 4 points for the flat-window turret for one elevation angle and 4 points for the hemisphere, also along the center-plane. In other studies, optical measurements around a flat-window turret were also taken [32], but due to lack of information about the turret size and other testing parameters it was impossible to re-scale and present them in Fig. 7. No doubt, significantly more experimental data are required to completely quantify and understand the optical environment around turrets for different elevation and azimuthal angles, even at low subsonic speeds.

3.3. Unsteady jitter

A few words should be said about the unsteady line-of-sight jitter imposed on the outgoing beam. For real turrets, the jitter always consists of the two parts. The aero-optically induced jitter is caused by the unsteady density variations around the turret. In addition to that, the unsteady pressure and velocity fluctuations create unsteady forcing on the turret, which, due to aero-elastic coupling, leads to a mechanically induced jitter of the turret itself, which can, in turn, excite jitter disturbances in the optical beam train including the telescope inside the turret. The summation of all these jitter contributions is eventually imposed on the outgoing beam. This jitter is especially damaging for the turrets with flat windows, since the flow around the turret is not symmetrical about the vertical axis.

Mechanically induced vibration almost always corrupts experimental measurements of the aero-optical jitter and in general it is difficult to separate them to get reliable aero-optical jitter data. Only in some cases when, for example, the mechanical jitter is separated from the aero-optical jitter in the frequency domain, it is possible to decouple them using high-speed wavefront sensors with sufficient temporal resolution.

3.4. Transonic and supersonic regimes

The above discussion of the flow topology and optical distortions caused by turrets is valid only for the fully subsonic regime, where the flow around the turret is subsonic everywhere. Since the flow accelerates over the turret, the local Mach number will reach a sonic value at some critical incoming Mach number. For incoming Mach numbers above the critical Mach number the flow will become locally supersonic.

Assuming isentropic flow, the C_p as a function of the local Mach number can be derived from the compressible Bernoulli equation as

$$C_p(M)=\frac{2}{\gamma M_\infty^2}\left[\left(\frac{1+((\gamma-1)/2)M_\infty^2}{1+((\gamma-1)/2)M^2}\right)^{\gamma/(\gamma-1)}-1\right] \tag{9}$$

If the incompressible pressure distribution C_{p0} is known, it is possible to estimate the local compressible C_p using a compressible Karman–Tsien correction [33]

$$C_P=\frac{C_{P0}}{\sqrt{1-M_\infty^2}+\left(\frac{M_\infty^2}{1+\sqrt{1-M_\infty^2}}\right)\frac{C_{p0}}{2}} \tag{10}$$

Combining these two equations, the critical incoming Mach number, M_{cr}, can be computed for the flow to reach the sonic speed at a given location with the incompressible C_{p0} value. From Fig. 5, the lowest C_{p0} on the turret is approximately -1.25, giving the critical incoming Mach number of 0.55. At this incoming Mach number the flow reaches the sonic speed on top of the turret. Above this critical Mach number, a local supersonic region will form on top of the turret with an ending normal shock. The boundary-layer-shock interaction will cause the flow to prematurely separate on top of the turret and form a larger separation region, as schematically indicated in Fig. 8, left. When the incoming Mach number increases further, the supersonic region on the turret will grow in size and extend to the base of the turret. The wake has the $C_{p0}=-0.3$, so it becomes fully supersonic at the incoming Mach number of 0.77.

Of course, this simple analysis does not take into account the turbulent wake behind the turret, so the real flow around the turret at transonic speeds is even more complex, with unsteady pockets of supersonic flows and weak shocks appearing in the wake; see Fig. 8, left.

The shock on top of the conformal turret has no fixed point to "anchor" itself and it oscillates rapidly due to the shock-boundary-layer interaction [34], thus adding another layer of unsteadiness to an already complex picture of the unsteady wake and imposing even higher levels of unsteady optical aberrations on the outgoing laser beam. There is a significant amount of work done to characterize the shock-boundary-layer interaction, yet to

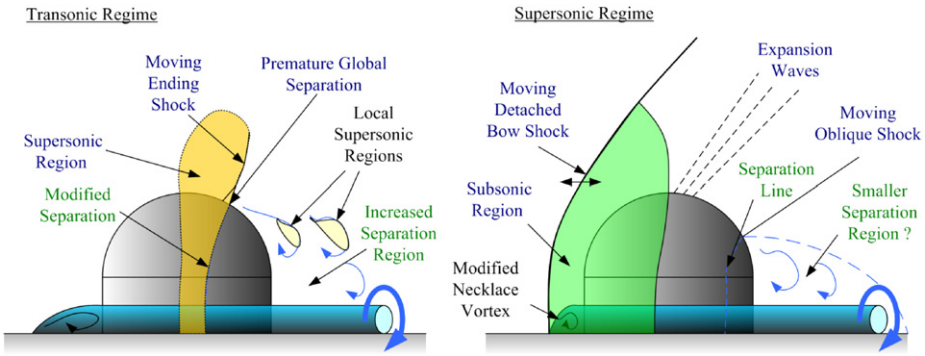

Fig. 8. Schematic of the flow around the turret at (left) transonic ($1 > M > M_{cr}$) and (right) supersonic ($M > 1$) speeds.

authors' knowledge, no direct optical data are available to quantify oscillating-shock optically aberrating effects.

The premature separation, a larger wake for transonic regime and increased density variations across the oblique shock and in the turret wake will undoubtedly impose higher than 'ρM^2'-predicted levels of optical aberrations on the outgoing laser beam at transonic speeds. This effect was experimentally measured for the case of the flow around the hemisphere [18]. It was shown that optical aberrations follow 'ρM^2'-law for incoming Mach numbers up to 0.5. At higher incoming, yet subsonic speed of $M=0.64$ the level of optical aberrations was found to be almost twice higher than the subsonic 'ρM^2'-law predicts. As it was mentioned above, this increase is due to the unsteady normal shock forming on top of the hemisphere, forcing premature separation and a larger turbulent wake downstream of the hemisphere. The normal shock was observed to rapidly move on top of the hemisphere at high frequencies of several kilohertz, but no quantitative data were taken.

When the incoming flow is supersonic, a detached bow shock forms in front of the turret and it modifies the formation of the necklace vortex at the bottom of the turret. The flow between the base of the turret and the bow shock is subsonic, but it quickly accelerates along the front portion of the turret, reaching sonic speed on top and becoming supersonic on the aft portion of the turret, see Fig. 8, right. The flow forms a series of weak expansion waves on top of the turret and eventually the normal shock forces the flow to separate on the back of the turret. There is some evidence that the turret wake might be smaller and closer to the base plate than in the case of fully subsonic flow. All shocks and expansion waves clearly introduce large density gradients into the flow, thus imposing significantly higher levels of steady lensing, unsteady jitter and higher-order components on the outgoing laser beam. No experimental data of optical distortions around turrets at supersonic speeds are available in open literature; this is largely because the hemisphere-on-cylinder turret concept becomes largely impractical at supersonic speeds due to significant increase in the steady/unsteady lift/drag caused by the turret, as well as much higher levels of optical distortions due to various aberrating factors as discussed above.

As a final note, preliminary studies performed at the Air Force Academy suggest that it might be possible to design a partially protruding, less-disturbing turret or "blister" with a stabilized front attached oblique shock, the minimized expansion wave on top of the "blister" and a reduced separation region as a possible turret configuration at supersonic speeds.

4. Effect of flow control on optical distortions

As discussed in the previous Section, unsteady optical aberrations are significant for large turrets at subsonic speeds and large

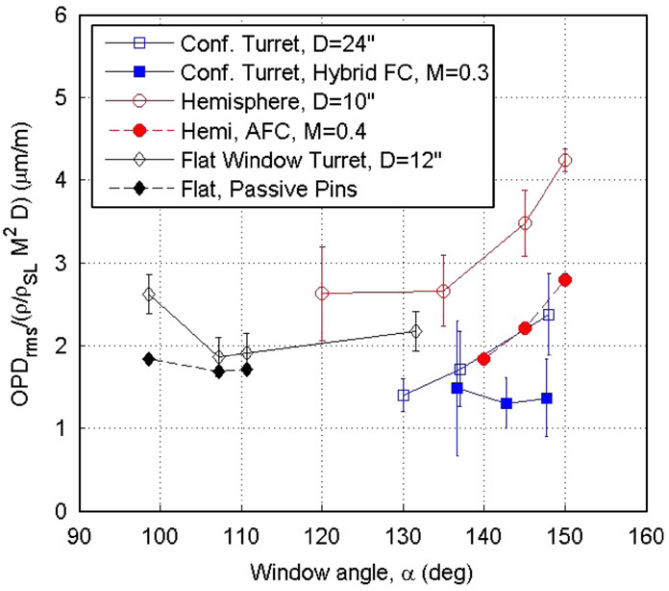

Fig. 9. Effect of different passive or active flow control (AFC) devices on the level of optical distortions, OPD_{rms}, normalized by $(\rho/\rho_{SL})M^2D$ for different turrets as a function of the window angle, defined in Eq. (1): conformal-window turret, $D=24''$, center-plane, baseline and with hybrid (passive+active) flow control (from [31]), hemisphere, $D=10''$, center-plane, baseline and with AFC (synthetic jets upstream of the window) (from [18]), flat-window turret, $D=12''$, baseline and passive pins upstream of the window, elevation angle is 30° (from [27]). Aperture size is 1/3 of the turret diameter for all cases.

back-looking angles. As an example, consider a laser beam directed at a window angle of 150° from the least-aberrating conformal-window turret with $D=1$ m flying at a sea-level at a relatively low speed of $M=0.3$. From Fig. 6 experimental data for conformal-window turrets give $A=1.05$ μm/m. Using Eq. (8), the level of optical aberrations would be $OPD_{rms}=0.18$ μm and the far-field time-averaged Strehl ratio (Eq. (1)) for $\lambda=1$ μm is found to be $SR=0.27$. In other words, more than 70% of the diffraction-limited laser intensity on a target will be lost.

The main source of large optical distortions is the separated turbulent region downstream the turret and one way to mitigate aero-optical problems and to increase the far-field Strehl ratio is to reduce the separation region or modify it to make it less optically active. This can be accomplished with either passive or active flow control.

A variety of different passive flow-control devices have been tested to minimize the separation region. They include fairings behind the turret, which are known to reduce aerodynamic drag, but were largely ineffective in significantly improving the aero-optical problem [35]. Fairings were also used to provide steady

suction behind the turret to reduce wake unsteadiness [36,37]; while some flow improvements were achieved, no optical measurements were present.

The flat-window aperture is generally cheaper to manufacture than the more expensive conformal-window aperture. But, as discussed above, the slope discontinuity around the flat-window aperture forces a premature separation over the flat-window aperture for side- and back-looking angles and consequently, creates a larger turbulent wake with higher levels of optical distortions, as demonstrated in Fig. 7. Early experiments [1] tested different fence arrangements and vortex generators upstream of the aperture on a flat-window turret in an attempt to delay the natural separation off the upstream slope discontinuity around the flat-window aperture; while these simple passive flow control devices can be easily implemented, they provide only marginal reductions in optical distortions at large back-looking angles.

Recently, it was discovered that at moderate back-looking angles a weak separation bubble is formed over the flat-window flow, which in turn results in significant increase in OPD_{rms} at these angles [27]. When a single row of small pins was placed upstream of the window, the pins energized the boundary layer and forced the flow to re-attach, reducing the separation bubble over the flat window and concomitantly lowering the levels of optical distortions at window angles up to 110° [27], see Fig. 9. Ongoing work on tall pins placed upstream of the flat-window shows some promising results in reducing optical aberrations at even higher window angles [38].

The flow over the conformal-window turret separates around 120° and generally is less aberrating than the flow over the flat-window turret. However, at large back-looking angles, levels of optical distortions can be significant for large turrets even at moderate Mach numbers, see Fig. 7.

Several flow control strategies were tested in order to reduce the size of the turbulent wake. One way to do it is to modify the flow locally and to delay the flow separation. Passive "fences" on top of the nose-mounted turret have been shown to improve the local C_p-distribution leading to significantly suppressing the shear layer formation in the cut-out behind the nose-mounted turret [40]. Additionally, these 'fences' were shown to increase the critical Mach number and keep the flow around the nose-mounted turret fully subsonic up to the incoming Mach number of 0.8.

High-frequency actuation of the flow just upstream of the separation line was shown to be effective in delaying flow separation over bluff bodies [41,42] and a variety of compact and powerful active-flow-control devices are now available. Rows of synthetic jets pulsating at high frequencies [43] were used upstream of the window on a hemisphere-only for low, up to $M=0.2$, [44,45] and high, up to $M=0.5$, subsonic speeds [18]; the actuators were shown to effectively delay the separation point and significantly improve optical distortions at relatively large back-looking angles [18]. Fig. 9 presents normalized levels of optical aberrations for the baseline (no actuation) and controlled cases (with synthetic jet actuation) in the hemisphere-only tests [18]. The optical environment behind the hemisphere was reduced by as much as 40% for the controlled cases. Similar tests over the conformal-window turret with the high-frequency actuations gave 5–30% improvement over a range of Mach numbers between 0.3 and 0.5 [30].

One important comment about using blowing-based actuators to control the flow around the turret should be made. If the injected gas has a different index-of-refraction value, like hot/cold air, hot plasma or different gas specie like helium, it will introduce its own optical distortions, which might negate the positive effects from the actuator on the flow. Therefore, the whole class of powerful actuators, like combustion actuators [46,56,57] and plasma-based actuators [47], for example, while been reported to significantly delay the separation and improve wakes behind airfoils and bluff bodies, will inject a higher-enthalpy gas into the flow and potentially introduce severe optical distortions due to the index-of-refraction mismatch between the flow and the gas introduced by the actuator. As such, care should be taken when choosing or designing actuators to mitigate aero-optical effects to make sure that they use a matching gas of the same total enthalpy. The above mentioned synthetic jets are blowing/suction, zero-net-mass type of devices, they use the ambient air as a working media without changing the air's total enthalpy and thus are free of the mismatched index-of-refraction problem.

Another way to modify the turbulent wake is to modify the necklace vortex formed at the bottom of the turret and favorably change the wake size. One potentially promising passive flow control device, a forward partition plate placed upstream the conformal-window turret has been shown to introduce a second necklace vortex; this additional vortex interacts with the main necklace vortex, forcing a delay in the separation point by more than 15° [39] and subsequently reducing optical distortions at high window angles up to 150° [31]. Further improvements can be achieved by hybrid flow control, i.e., by combining passive and active flow controls. The combination of the partition plate and active-flow control actuators provided up to a 40% reduction in levels of aero-optical aberrations over the conformal-widow turret at the viewing angles as high as 148° at $M=0.3$ and $Re_D=4.5\times10^6$, [31], see Fig. 9. Returning to the example used in the beginning of this Section, if hybrid flow controls [31] were used, the OPD_{rms} would be reduced to 0.116 μm and the Strehl ratio would increase up to 0.58, a factor-of-two improvement in the far-field intensity.

Passive flow control, if effective, is the more attractive choice, because it generally does not require any moving parts and the energy to control the flow is drawn from the flow itself; furthermore, because the energy is drawn from the flow passive approaches tend to be equally effective over a large range of Reynolds and Mach numbers. Active flow-control typically introduces a fixed amount of the energy into the flow, therefore their effectiveness decreases with increase in Reynolds number, and it usually requires an external power source. Finally, depending on the device, active flow actuators are generally placed inside the turret, further complicating the turret assembly. On the other hand, active-flow control devices, unlike passive flow control devices, can be tuned for different flow regimes.

As a final remark on active flow control approaches, several *closed-loop*, active-flow-control algorithms were recently developed [48,49]. They use unsteady pressure sensors placed on the surface of the flat-window turret as a feedback into a POD-based model to drive pulsating synthetic jets upstream of the window. The closed-loop control algorithm was designed to reduce surface pressure fluctuations. No direct optical data are available yet, but the levels of surface unsteady pressure, which are believed to be linked to optical aberrations [17], were reduced by 18% and it was observed that the actuation drives the flow toward homogeneity. Another interesting experimental study used a laser-induced spark as a beacon to instantaneously measure and compensate aero-optical effects caused by a compressible shear layer using a feed-forward, adaptive-optic system [50].

5. Computational efforts to predict the fluid dynamics and aero-optical aberrations of turrets.

Aero-optical problems are computationally difficult, because they are required to properly resolve small-scale unsteady fluctuations in the flow. The flow around a turret is particularly

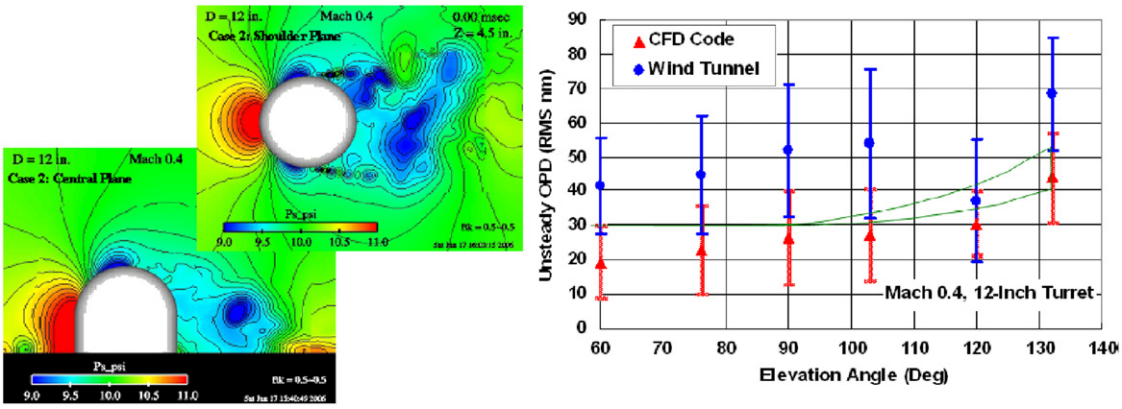

Fig. 10. Left: snapshots of flow-field around the turret (from [16]). Right: comparison of levels of optical aberrations between experiments [17] and CFD [16].

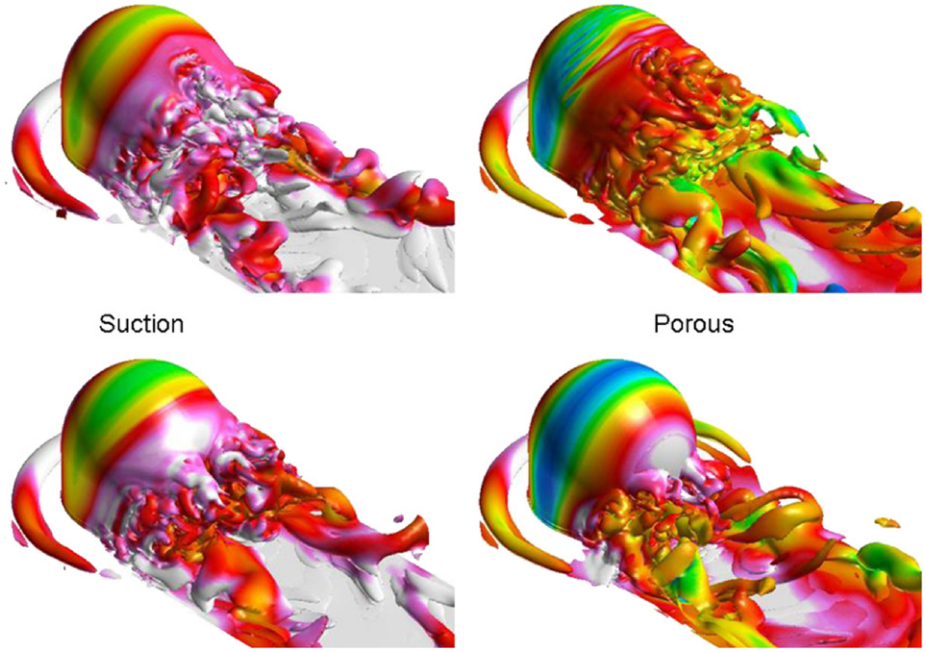

Fig. 11. Numerical simulations of the flow around the turret and effects of porous suction (from [53]).

computationally challenging, since it has a large range of vortical structures that must be properly resolved; these structures range in scale from the order of the turret diameter (the necklace vortex and the separation region) down to small vortical structures in the separated shear layer. The density field must be resolved both temporally and spatially, so steady RANS models cannot be used. Also, typical Reynolds numbers for turrets are in the millions and direct numerical simulations (DNS) would require a prohibitive amount of computational resources to compute the flow.

This review is mostly focused on experimental studies of aero-optical properties of turrets, as computational fluid dynamics is outside the scope of authors' experience. Therefore, we will provide only a very short review of computational efforts in this area.

In one of the first attempts [51] to calculate the unsteady compressible flow around a turret, a Cebeci–Smith type eddy viscosity model was used to solve the unsteady N–S equations. In a different study [19], the unsteady density field around a partially protruding hemisphere with a flat window was computed from the CFD analysis and used to perform aero-optical analysis of laser beams propagating from the turret. The flow around a nose-mounted turret was computationally studied in [10].

Recently, several LES-based codes were tailored to flow around turrets and validated against experimental results. A CFD-based validation study using a k–ε turbulence model with an unsteady partially averaged Navier–Stokes (PANS) solver was conducted [16]; this study was shown to correctly predict aerodynamic and aero-optical environment around small and large conformal-window turrets, see Fig. 10. An implicit large-eddy-simulation (ILES), 6th-order solver was developed [52], which favorably compared to experiments [17]. Many features of the flow were properly predicted, although some differences were noted in the separation region. A modification of this code, a hybrid RANS/ILES solver [53] was used to predict the flow around a conformal-window turret at $M=0.4$ and $Re_D=2.4\times10^6$. This code was also used to test the effectiveness of different suction strategies on the turret, see Fig. 11. An unsteady Reynolds-averaged Navier–Stokes (RANS) model and a blended large eddy simulation (LES) with a two-equation turbulence model [14] were evaluated to predict aerodynamics and aero-optics of the turrets. Aerodynamic predictions of time-averaged turret surface pressures and several

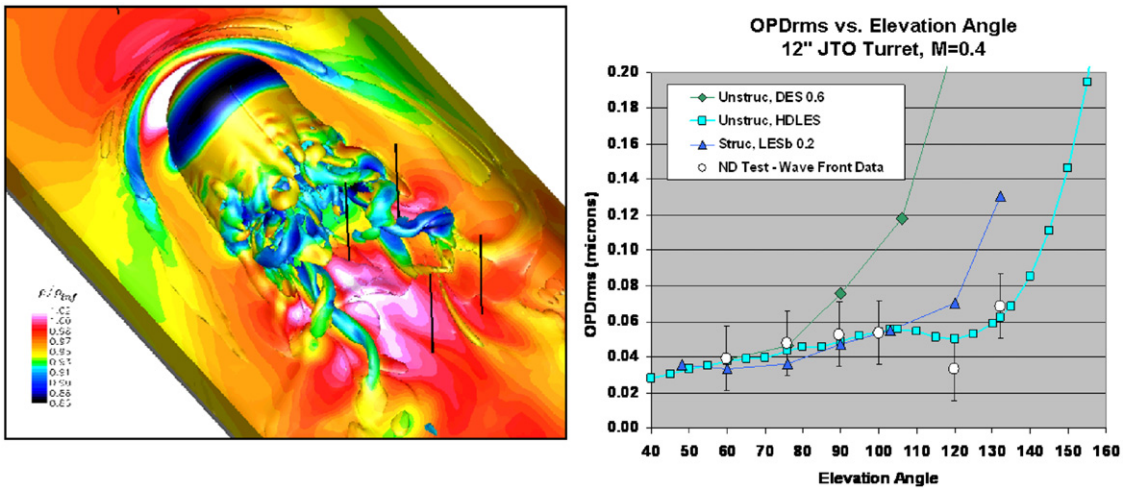

Fig. 12. Left: flow around the turret with a conformal window. Right: comparison of OPDrms with experiments (from [14]).

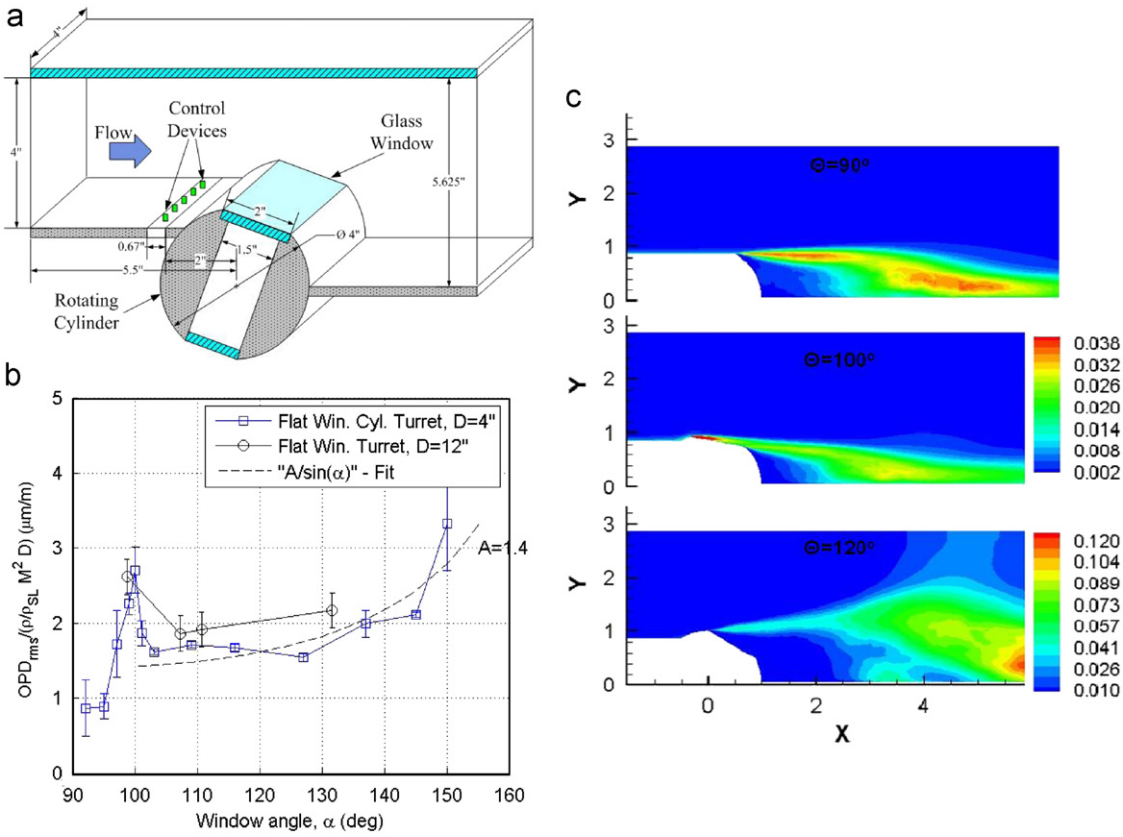

Fig. 13. (a) Schematic of the cylindrical turret with the flat window, (b) comparison of the optical data between the cylindrical turret, $D=4''$ (from [25]) and the flat-window turret, $D=12''$, $H/D=0.375$, $\gamma=30^\circ$ (from [27]), (c) computational time-averaged kinetic-energy contours around the cylindrical turret (from [55]).

downstream velocity profiles showed good agreement with experiments. These time-averaged results not only compared well with surface-flow visualization, but as mentioned in Section 2 helped evolve our understanding of the complicated flow field in the wake. The results shown in Fig. 11, which represent instantaneous realizations of the unsteady solution, point out the complexities in the flow a laser beam must traverse. Aero-optical quantities also compared well with experiment through a range of elevation angles, see Fig. 12. It is important to mention that steady-state solutions, while been computationally easier, are often quite different from time-averaged solutions; so, it is not even helpful to compare surface flow visualization to steady-state solutions.

Almost all cited CFD studies dealt with flow around conformal-window, hemisphere-on-cylinder turrets, which do not depend on the viewing angle; thus, the same numerical solution can be used to calculate the optical distortions at different viewing angles, since it only requires post-integrating along different beam directions. The flat-window turret, on the other hand, requires a

separate numerical simulation for each viewing angle, thus making the computational predictions very expensive. To the authors' knowledge, there are no available numerical simulations, except for [19] that predict aero-optics of flat-window turrets at realistic Reynolds numbers.

6. Cylindrical turret

To finish our discussion of aero-optical environment around turrets, it is important to note that due to geometrical simplicity and relevance to aero-optical problems [27], the experimental results for the flow and aero-optical aberrations around a two-dimensional, cylindrical turret [25,26] provide excellent benchmark experimental data to test different passive flow control devices and to validate CFD studies. Aero-optical results for the cylindrical turret with a flat window are presented in Fig. 13 and they were also found to follow the "$1/\sin(\alpha)$" approximation with $A=1.4$ μm/m. Moreover, as discussed in detail in [27], the aero-optical environment around a simplified 2-D flat-window turret is quite similar and relevant to the environment around a 3-D flat-window hemisphere-on-cylinder turret, which is also presented in Fig. 13; the two share the same unsteady source of the optical aberrations—a separated flow over the flat-window. Therefore, the flow around the cylindrical turret with the flat window becomes an important benchmark experiment to validate different aero-optical computational codes [54,55].

7. Conclusions

This paper is really a first attempt at trying to bring together what is now known about airborne optical turrets; as such, there is bound to be information we have overlooked. The data presented here represents all of the open-literature data known to us on the fluid dynamics and aero-optics associated with canonical hemisphere-on-cylindrical-base turrets, including the case where the cylinder height of the base is zero, i.e., a hemisphere-only turret. The turret types include flat-windowed turrets, where the optical window's edge blends into the hemisphere with an abrupt slope discontinuity, and conformal-windowed turrets, where the window itself has a spherical outer surface of the same radius as the rest of the hemisphere. These data range in Reynolds number based on the turret diameter from less than 300,000 up to several million; the nominal transition of the boundary layer just prior to separation changing from laminar to turbulent is around 300,000. These data also range in Mach number from around 0.3 to 0.65; somewhere between Mach 0.5 and 0.65, shocks form on the turrets, at which point the inferences and scaling rules presented in this paper break down and no longer apply. It is clear that even after decades of studying this problem, there is a paucity of data; a simple title search for the word "turret" in the AIAA database, for example, revealed 6 papers prior to 1983, no papers between 1984 and 1999, and then a burst of publication in the last few years, with 24 papers in the last three years alone. With the new emphasis on using turrets to project relatively short-wavelength lasers ($\sim$1 μm) from aircraft, it is clear that studies of the kind reviewed in this paper must continue so that a fuller understanding of the effects over the full field of regard is available to airborne-laser system designers. A clear message contained in the data reviewed here is that design by intuition is bad practice, as evidenced by the fact that the worst turret reported was for the hemisphere-only turret.

It is also clear that a little flow control goes a long way in improving the optical environment over otherwise canonical turrets. As was noted in Section 1, aero-optics encompasses more than just the tilt-removed aberrating wavefront effects; it includes aero-induced, line-of-sight jitter and shock-related effects. In this regard, recently work has begun to address the latter two aero-optic effects, and we hope someday to be able to gather these efforts together for a future review. While some day we may have optical windows that not only conform to the outer shape of an aircraft without themselves distorting the beam and with antireflective coatings that allow for no energy to be reflected back in all directions that depend on the angle the beam is projected through them, today the most viable projection direction is still perpendicular to the window. This means that turrets of the form we have discussed in this paper will continue to be prime candidates for projecting lasers from aircraft. The solution then does not appear to be looking for a different turret shape, but rather using passive and active flow control to fool the flow going over the turret into thinking that it is going around an aerodynamically optimized shape. There is clearly much work to be done.

References

[1] Gilbert KG, Otten LJ, editors. Aero-optical phenomena, Progress in astronautics and aeronautics series, vol. 80. New York: American Institute of Aeronautics and Astronautics; 1982.
[2] Tatarskii VI, Zavorotnyi VU. Wave propagation in random media with fluctuating turbulent parameters. J Opt Soc Am A 1985;2(12):2069–76.
[3] Sutton GW. Aero-optical foundations and applications. AIAA J 1985;23:1525–37.
[4] Jenkins F, White H. Fundamentals of optics. 4th ed.. McGraw-Hill; 1976.
[5] Gladstone JH, Dale TP. Researches on the refraction, dispersion, and sensitiveness of liquids. Philos Trans R Soc London 1863;153:317–43.
[6] Gardiner Jr WC, Hidaka Y, Tanzawa T. Refractivity of combustion gases. Combust. Flame 1980;40:213–9.
[7] Smith WJ. Modern optical engineering: the design of optical systems. New York: McGraw-Hill; 1966 Chapter 3, p. 49–71.
[8] Gordeyev S, Hayden T, Jumper E. Aero-optical and flow measurements over a flat-windowed turret. AIAA J 2007;45(2):347–57.
[9] Abado S, Gordeyev S, Jumper E. Two-dimensional high-bandwidth Shack-Hartmann wavefront sensor: design guidelines and evaluation testing. Opt Eng June 2010;49(6):064403.
[10] Pond J, Sutton G. Aero-optic performance of an aircraft forward-facing optical turret. J Aircr 2006;43(3):600–7.
[11] Gordeyev S, Jumper E. Fluid dynamics and aero-optical environment around turrets. In: Proceedings of the 40th AIAA plasmadynamics and lasers conference, San-Antonio, TX, 22–25 June, 2009. AIAA Paper 2009–4224.
[12] Achenbach E. Experiments on the flow past spheres at very high reynolds numbers. J Fluid Mech 1972;54(3):565–75.
[13] Sluder R, Gris L, Katz J.. Optical turret aerodynamics—a preliminary study. In: Proceedings of the 46th AIAA aerospace sciences meeting and exhibit, 2008. AIAA Paper 2008-429.
[14] Ladd J, Mani M, Bower W. Validation of aerodynamic and optical computations for the flow about a cylindrical/hemispherical turret. San-Antonio: AIAA; 2009. Paper 2009-4118.
[15] Vukasinovic B, Glezer A, Gordeyev S, Jumper E, Kibens V. Fluidic control of a turret wake, part I: aerodynamic effects. In: Proceedings of the 47th aerospace science meeting and exhibit, Orlando, FL, 5–8 January, 2009. AIAA Paper 2009-0816.
[16] Nahrstedt D, Hsia Y-C, Jumper E, Gordeyev S, Ceniceros J, Weaver L, DeSandre L, McLaughlin T. Wind tunnel validation of computational fluid dynamics-based aero-optics model. Proc. IMechE Part G: J Aerosp Eng 2009;223(G4):393–406.
[17] Gordeyev S, Post M, MacLaughlin T, Ceniceros J, Jumper E. Aero-optical environment around a conformal-window turret. AIAA J 2007;45(7):1514–24.
[18] Vucasinovic B, Glezer A, Gordeyev S, Jumper E, Kibens V. Active control and optical diagnostics of the flow over a hemispherical turret. In: Proceedings of the 46th aerospace science meeting and exhibit, 2008. AIAA Paper 2008-0598.
[19] Jones MI, Bender EE.CFD-based computer simulation of optical turbulence through aircraft flowfields and wakes. In: 32nd AIAA plasmadynamics and lasers conference, Anaheim, CA, June 11–14, 2001. AIAA Paper 2001-2798.
[20] Tyson RK. Principles of adaptive optics. San Diego: Academic Press, Inc.; 1991.
[21] Fuhs AE, Fuhs SE. Optical phase distortion due to compressible flow over laser turrets. In: Gilbert KG, Otten LJ, editors. Aero-optical phenomena, vol. 80, Progress in astronautics and aeronautics, New York: AIAA; 1982. p. 101–38.
[22] Wittich D, Gordeyev S, Jumper E. Revised scaling of optical distortions caused by compressible, subsonic turbulent boundary layers. In: Proceedings of the

38th AIAA plasmadynamics and lasers conference, Miami, Florida, 25–28 June, 2007. AIAA Paper 2007-4009.
[23] Cress J, Gordeyev S, Post M, Jumper E. Aero-optical measurements in a turbulent, subsonic boundary layer at different elevation angles. In: Proceedings of the 39th plasmadynamics and lasers conference, Seattle, Washington, 23–26 June, 2008. AIAA Paper 2008-4214.
[24] Cress J, Gordeyev S, Jumper E. Aero-optical measurements in a heated, subsonic, turbulent boundary layer. In: Proceedings of the 48th aerospace science meeting and exhibit, Orlando, Florida, 4–7 January, 2010. AIAA Paper 2010-0434.
[25] Gordeyev S, Jumper E, Ng T, Cain A. The optical environment of a cylindrical turret with a flat window and the impact of passive control devices. In: Proceedings of the 36th AIAA plasmadynamics and laser conference, Toronto, Canada, 6–9 June, 2005. AIAA Paper 2005-4657.
[26] Gordeyev S, Cress JA, Jumper E, Cain AB. Aero-optical environment around a cylindrical turret with a flat window. AIAA J, Submitted for publication.
[27] Cress J, Gordeyev S, Jumper E, Ng T, Cain A. Similarities and differences in aero-optical structure over cylindrical and hemispherical turrets with a flat window. In: Proceedings of the 45th aerospace science meeting and exhibit, Reno, Nevada, 8–11 January, 2007. AIAA Paper 2007-0326.
[28] Fitzgerald EJ, Jumper EJ. The optical distortion mechanism in a nearly incompressible free shear layer. J Fluid Mech 2004;512:153–89.
[29] Duffin D. Feed-forward adaptive-optic correction of a weakly-compressible high-subsonic shear layer. PhD thesis, University of Notre Dame, Notre Dame, IN, 2009.
[30] B. Vukasinovic, A. Glezer, S. Gordeyev, E. Jumper and V. Kibens, Fluidic control of a turret wake: aerodynamic and aero-optical effects. AIAA J, 2010; 48(8):1686–1699.
[31] Gordeyev S, Jumper E, Vukasinovic B, Glezer A, Kibens V. Hybrid flow control of a turret wake, part II: aero-optical effects. In: Proceedings of the 48th aerospace science meeting and exhibit, Orlando, Florida, 4–7 January, 2010, AIAA Paper 2010-0438.
[32] Craig JE, Trolinger JD, Rose WC. Propagation diagnostic technique for turbulent transonic flow. AIAA Paper 84-0104, January 1984.
[33] Shapiro AH. The dynamics and thermodynamics of compressible fluid flow, vol. 1. Ronald Press; 1953.
[34] Smits AJ, Dussauge J-P. Turbulent shear layers in supersonic flow. 2nd ed.. New York: Springer; 2006.
[35] Otten LJ, Gilbert KG. Inviscid flowfield effects: experimental results. In: Gilbert KG, Otten LJ, editors. Aero-optical phenomena, vol. 80, Progress in astronautics and aeronautics, New York: AIAA; 1982. p. 233–41.
[36] Schonberger JR, Fuhs AE, Mandigo AM. Flow control for an airborne laser turret. J Aircr 1982;19(7):531–7.
[37] Purohit SC, Shang JS. Effect of suction on the wake structure of a three-dimensional turret. In: 16th fluid and plasmadynamics conference, Danvers, MA: American Institute of Aeronautics and Astronautics; July 12–14, 1983. AIAA Paper 1983-1738.
[38] Cress J, Gordeyev S, Smith A, Jumper E. Improvement in optical environment over turrets with flat window using passive flow control. In: Proceedings of the 41st plasmadynamics and lasers conference, Chicago, IL, June 28–July 1, 2010. AIAA-2010-4492.
[39] Vukasinovic B, Glezer A, Gordeyev S, Jumper E, Kibens V. Hybrid flow control of a turret wake, part I: aerodynamic effects. In: Proceedings of the 48th aerospace science meeting and exhibit, Orlando, Florida, 4–7 January, 2010. AIAA Paper 2010-0086.
[40] Rennie M, Crahan G, Jumper E. Aerodynamic design of an aircraft-mounted pod for improved aero-optic performance. In: Proceedings of the 48th AIAA aerospace sciences meeting, Orlando, Florida, January 4–7, 2010. AIAA Paper 2010-0437.
[41] Smith DR, Amitay M, Kibens V, Parekh D, Glezer A. Modification of lifting body aerodynamics using synthetic jet actuators. AIAA Paper 1998-0209, 1998.
[42] Amitay M, Glezer A. Role of actuation frequency in controlled flow reattachment over a stalled airfoil. AIAA J 2002;40:209–16.
[43] Smith BL, Glezer A. The formation and evolution of synthetic jets. Phys Fluids 1998;10:2281–97.
[44] Vukasinovic B, Brzozowski D, Glezer A, Bower WW, Kibens V. Separation control over a surface-mounted hemispherical shell. AIAA Paper 2005-4878.
[45] Vukasinovic B, Glezer A. Control of a separating flow over a turret. AIAA Paper 2007-4506.
[46] Crittenden TM, Raghu S. Combustion powered actuator with integrated high frequency oscillator. Int J Flow Control 2009;1(1):87–97.
[47] Corke TC, Post ML, Orlov DM. Single dielectric barrier discharge plasma enhanced aerodynamics: physics, modeling and applications. Exp Fluids 2009;46:1–26.
[48] Wallace R, Andino M, Glauser M, Camphouse R, Schmit R, Myatt J. Flow and aero-optics around a turret, part II: surface pressure based proportional closed loop flow control. In: Proceedings of the 39th plasmadynamics and lasers conference, Seattle, Washington, June 23–26, 2008. AIAA Paper 2008-4217.
[49] Wallace R, Andino M, Glauser M, Camphouse C, Schmit R, Myatt J. Flow characteristics of active control around a 3D turret. In: Proceedings of the 47th AIAA aerospace sciences meeting, Orlando, Florida, January 5–8, 2009. AIAA Paper 2009-573.
[50] Rennie M, Cavalieri D. Jumper E, Goorskey D, Whiteley M. Optical measurements of a compressible shear layer using a laser-induced air breakdown beacon. In: Proceedings of the 48th AIAA aerospace sciences meeting, Orlando, Florida, January 4–7, 2010. AIAA Paper 2010-1158.
[51] Purohit SC, Shang JS, Hankey, Jr. WL. Numerical simulation of flow around a three-dimensional turret. In: Proceedings of the 3rd AIAA and ASME, joint thermophysics, fluids, plasma and heat transfer conference, St. Louis, MO, June 7–11, 1982. AIAA Paper 1982-1020.
[52] Morgan P, Visbal M. Large eddy simulation of flow around a turret. In: Proceedings of the 38th fluid dynamics conference and exhibit, Seattle, WA, June 23–26, 2008. AIAA Paper 2008-3749.
[53] Morgan PE, Visbal MR.Numerical simulations investigating control of flow over a turret. In: Proceedings of the 47th AIAA aerospace sciences meeting, Orlando, Florida, January 5–8, 2009. AIAA Paper 2009-574.
[54] Wang K, Wang M. Numerical simulation of aero-optical distortions by flow over a cylindrical turret. In: Proceedings of the 40th AIAA plasmadynamics and lasers conference, San-Antonio, TX, June 22–25, 2009. AIAA Paper 2009-4223.
[55] Morgan PE, Visbal M. Large eddy simulation of flow over a flat-window cylindrical turret with passive flow control. In: Proceedings of the 48th Aerospace Science Meeting and Exhibit, Orlando, FL, 4–7 January, 2010. AIAA Paper 2010-0916.
[56] Woo G, Crittenden T, Glezer A. Transitory control of a pitching airfoil using pulse combustion actuation. In: Proceedings of the 4th AIAA flow control conference, Seattle, WA, June 2008. AIAA Paper 2008-4324.
[57] Woo G, Crittenden T, Glezer A. Transitory separation control over a stalled airfoil. In: Proceedings of the 39th AIAA fluid dynamics conference, San Antonio, TX, June 2009. AIAA Paper 2009-4281.
[58] Ross TS. Limitations and applicability of the Maréchal approximation. Appl Opt 2009;48(10):1812–8.